Journal of Zhejiang University-SCIENCE A 2025 26(12):1141-1162
www.jzus.zju.edu.cn; www.springer.com/journal/11582
E-mail: jzus_a@zju.edu.cn

Research Article
https://doi.org/10.1631/jzus.A2400343

Check for updates

Piezoelectric ultrasonic coupling-based polishing of micro-tapered holes with abrasive flow

Gaoan ZHENG[1,2], Xiaoxing WENG[1,4], Tong WANG[3], Pu XU[1], Weixin XU[1], Lin LI[1]✉, Xuefeng XU[1], Dapeng TAN[1]✉

[1]*College of Mechanical Engineering, Zhejiang University of Technology, Hangzhou 310014, China*
[2]*School of Mechanical Engineering, Zhejiang University of Water Resources and Electric Power, Hangzhou 310018, China*
[3]*College of Mechanical and Electrical Engineering, Jining University, Jining 273155, China*
[4]*Research Institute of Tea Resources Utilization and Agricultural Products Processing Technology, Zhejiang Academy of Agricultural Machinery, Jinhua 321017, China*

Abstract: The primary determinant of microfluidic chip performance is the surface quality of the micro-tapered holes. Due to the small scale of these holes and the high hardness of the surface attachments, the commonly used abrasive jet polishing method can encounter difficulties. Therefore, we propose a novel active multiphase field material removal technique. This technique is based on piezoelectric ultrasonically coupled abrasive particle flow. To study the connection between the impulse properties of the flow field and the micro-tapered hole's asymptotic expansion–contraction process, a multiphase hybrid fluid dynamics model is established. Simultaneously, we investigate the process of abrasive–wall contact during the cycles of expansion and contraction, revealing the effects of erosion and polishing on different areas of the hole surface. To achieve accurate regulation of a desired polishing area, a quantitative relationship between the vibrational properties of piezoelectric ceramics and the erosional effect of micro-tapered holes is established. Finally, an experimental platform for micro-tapered hole polishing is built to validate the method.

Key words: Abrasive flow finishing; Micro-tapered holes; Piezoelectric ultrasonic coupling-based polishing; Surface quality; Polishing efficiency

1 Introduction

Microfluidic chips are commonly used in pharmaceutical and chemical engineering to precisely manage fluids at a mesoscale level. They are utilized for tasks such as analyzing and detecting samples, delivering drugs, and releasing drugs in a controlled manner (Ramshani et al., 2019; Gao et al., 2023; Li et al., 2023a; Ma et al., 2023). Micro-tapered holes are the main locations where mesoscale fluids undergo mixing, reaction, and separation (Nakamura et al., 2020; Zhang et al., 2022; Wu et al., 2024b); moreover, they constitute the main structures of microfluidic chips. The surface quality of micro-tapered holes directly influences flow properties, mixing effects, and analytical sensitivities of mesoscopic fluids (Tadaki et al., 2017; Chen et al., 2020; Gao et al., 2020; Li L et al., 2022, 2024a; Liu et al., 2024). Therefore, refining the structure of micro-tapered holes is crucial for controlling mesoscale flow patterns within microfluidic chips. For example, atomizers in medical devices utilize metal sheets with clusters of micro-tapered holes to produce atomization. The roughness of the inner wall of these holes impacts the size of the conical holes, which in turn affects the size of the atomized particles (Li et al., 2020; Yan et al., 2021; Ge et al., 2024). Valveless piezoelectric micropumps in microfluidic chips exploit disparities in flow resistance between conical holes to generate differential fluid flow in a specific direction. In this case, the surface roughness of the inner walls of the conical holes can impact

✉ Lin LI, linli@zjut.edu.cn
Dapeng TAN, tandapeng@zjut.edu.cn
Lin LI, https://orcid.org/0000-0002-3308-7857
Dapeng TAN, https://orcid.org/0000-0002-6018-9648

Received July 3, 2024; Revision accepted Aug. 17, 2024;
Crosschecked Nov. 13, 2025; Online first Dec. 17, 2025

the rate of flow (Li K et al., 2022; Wang et al., 2023; Guo et al., 2024).

Micro and nano-micro cone holes are usually created through laser processing (Shin et al., 2020; Ji et al., 2024; Sun et al., 2024; Xu WX et al., 2025), and the characteristics of the holes are influenced by the processing procedure and heat. The walls of the resulting holes generally contain a re-solidified layer with a stepped-ring pattern, and are coated with black metal oxides due to the laser sintering, as depicted in Fig. 1. The irregular micro-tapered hole wall greatly increases the difficulty of material removal uniformity control. Energy spectrometers can be used to investigate ferrous metal oxides that stick to the hole walls, such as Cr_2O_3 and $FeCr_2O_4$ (Yang et al., 2024; Lin et al., 2025b). These oxides are often tough and tightly attached, making it difficult to polish the sidewall surfaces.

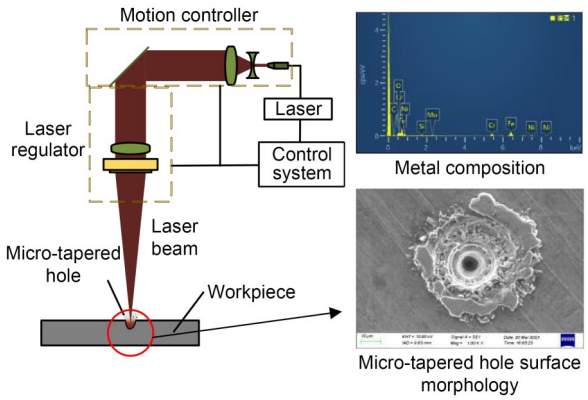

Fig. 1 Principle of laser processing of micro-tapered holes and their surface morphology

Present research on the polishing of micro-tapered holes often involves using ion beam polishing techniques (Xiao et al., 2021), electrochemical discharge microporous polishing (ECDM) (Zhang et al., 2020), and abrasive jet polishing (AJP) (Kowsari et al., 2014; Kim et al., 2020; Tan et al., 2023). Each of these approaches possesses distinct advantages and can yield superior surface quality depending on the specific subject to be polished. However, they also have limitations in their respective applications. The ion beam polishing technique involves directing a stream of ion beams towards the surface of a component, resulting in a sputtering effect that removes material (Deng et al., 2020; Peng et al., 2021). This helps achieve higher surface quality in desired micro-regions (Deng et al., 2019; Xiao et al., 2021). Nevertheless, the effectiveness of ion beam polishing for removing material is somewhat limited, and having precise control over the taper of tapered holes is challenging. Electrochemical discharge machining is a technique that utilizes electrical spark discharges to produce heat, which enables etching into the surface material of an object (Zhang et al., 2020). This method achieves polishing precision at the micron level and has found extensive application in the drilling of hard and brittle materials, like glass and ceramics. However, during the polishing of micro-tapered holes, the inner wall discharge can lead to heat-affected zones on the inner wall surface. Furthermore, difficulties in maintaining a continuous flow of electrolyte can lead to intermittent discharge, making it more challenging to achieve accurate depths and dimensions of small holes.

AJP is a fluid-based method that uses high-energy abrasives to erode and process materials (Kowsari et al., 2014; Li et al., 2021a, 2021b; Tan et al., 2023). This method has great flexibility and does not lead to heat-affected zones. The technique is commonly employed for microstructural and surface-polishing treatment of hard and brittle materials, such as ceramics, glass, and stainless steel, which are challenging to machine (Tong and Li, 2024; Zhang et al., 2024; Lin et al., 2025a). The AJP method utilizes a polishing medium consisting of fluid with micron-sized abrasive particles. This medium establishes effective contact with the target surface, enabling polishing through collisions between the abrasive particles and the surface. This method of contact has the ability to address challenges related to microstructure polishing, and also leads to better polishing uniformity. Shanu et al. (2024) reviewed the polishing of micro-scale hardened materials using the AJP technique, considering various abrasive characteristics. Their study revealed that the abrasive hardness and fracture toughness of the materials comprising the walls of micro-tapered holes are crucial parameters that influence AJP performance. Specifically, superior micromachining results are obtained when the abrasive hardness surpasses the hardness of the micro-tapered hole materials, such as boron nitride and artificial diamond, in comparison to the materials forming the walls of the micro-tapered holes. Painuly et al. (2023) examined the mechanism by which microchannels on high-pressure abrasive jet-polished 6061-T6 aluminum plates undergo surface evolution. Their goal was to uncover the correlation between the polishing effects and the size of the

stagnation zone, the behavior of bouncing abrasive grains, and the localized impact angle and velocity of abrasive grains. In another study, Feng et al. (2023) developed a novel technique called multiphase jet polishing to internally polish heat exchanger pipes with intricate designs. They discovered that the abrasive jets displayed selective removal of spherical protrusions on the inner surface of the pipes. This demonstrates the advantages of AJP in refining the interior surface of pipes with intricate configurations. The aforementioned investigations show how AJP can prevent additional harm to the side wall surface of micro-tapered holes, and can manipulate fluid parameters to achieve targeted polishing in desired regions. However, the standard AJP approach is not efficient at removing materials.

Ultrasonic assistance is a widely used technique that enhances the energy in a fluid (Kumar et al., 2021; Li L et al., 2024b, 2024c; Fu et al., 2025). By ultrasonically boosting a polishing fluid's kinetic energy within a microstructure, improved polishing efficiency can be achieved for micro-tapered holes in hard and brittle materials (Subramani et al., 2022; Li ZA et al., 2024; Yin et al., 2024). Qi et al. (2021) introduced an ultrasonic vibration-assisted AJP technique for treating micropores in K9 glass. Their study showed that ultrasound-assisted AJP technology can successfully control the path of abrasive particles, increase the frequency and intensity of collisions between the abrasive particles and the wall, and consequently improve the rate at which material is removed in the micro-structured flow field. Additionally, Ge et al. (2023) introduced a rapid polishing technique for glass microchannels using an ultrasonically coupled AJP method. Their findings demonstrated that ultrasonic vibration could enhance the turbulent kinetic energy and shock erosion of a mesoscale flow field. This effect is crucial for maintaining the stability of the jet and improving the efficiency of the polishing process. Moreover, Zhao et al. (2020) introduced a micro-millimeter-scale ultrasonic cavitation AJP technique for small and intricate optical surfaces. They discovered that ultrasonic cavitation can enhance the material removal rate by 380% while maintaining the same surface roughness.

Nevertheless, if the diameter of the micro-tapered holes is smaller than 10 μm (significantly smaller than the natural diameter through which fluid flows), it becomes challenging for high-energy fluids to pass through the pores rapidly (Fettiplace and Haydon, 1980; Chen et al., 2023; Li Z et al., 2024). The microfluidic chip contains a highly concentrated arrangement of micro-tapered holes, making it unfeasible to supply micro-pumps for each individual pore. Hence, to address polishing challenges for mesoscopic-scale micro-tapered holes, a novel method called active multiphase field material removal has been suggested. The method polishes micro-tapered holes through the piezoelectric ultrasonic coupled abrasive flow polishing (PU-AP). The operation principle of a valveless piezoelectric micropump (Tan et al., 2019, 2020; Lu et al., 2020; Shan et al., 2022) is employed to facilitate this process. The PU-AP process involves the periodic vibration of piezoelectric ceramics, causing the volume of the inner cavity of the micro-tapered hole to undergo a cyclic transformation. This leads to a strong coupling between the abrasive grain flow and the micro-tapered hole cavity, as caused by differential pressure. As a result, the inner wall surface of the micro- and nano-scale tapered holes experiences a pulsed impact, enhancing the turbulence intensity of the internal flow field through the micro-tapered hole and improving polishing efficiency.

In this study, we establish a fluid dynamics model that involves multiple phases and a mixture, based on PU-AP. This model allows us to understand the polishing principle of PU-AP and the formation mechanism of pulsed flow fields. By considering the wall boundary conditions, we can determine the trajectory of abrasive grains and the erosion effect on the wall surface of micro-tapered holes. This enables us to actively adjust the specific polishing area on the wall surface of these holes. Using the principles of PU-AP, we also developed equipment for better polishing of micro-tapered holes. To validate the effectiveness of our method, we used a 3D measuring laser microscope to obtain surface morphology and roughness measurements of the holes at different time points.

2 PU-AP theoretical model

2.1 Fluid mechanical model for PU-AP

During the process of the PU-AP, the abrasive particles within the flow field inside the micro-tapered holes collide with the wall in a pulsating fashion, due to the influence of ultrasound. Examining the properties of the flow field within a micro-tapered hole

requires considering the validity of the fluid continuity assumptions, vortex forms, and dissipation effects at the micro- and nano-scales (Li L et al., 2021b; Tan et al., 2024; Yan et al., 2024). Experiments have confirmed that pipes on the scale of micrometers and larger are still describable by traditional hydrodynamic theory (Li and Zheng, 2014). The micro-tapered holes in this study have a minimum size at the micron level, making the classical hydrodynamic theory applicable. Furthermore, the movement of the abrasive particles within the small tapered holes creates turbulence in specific areas, due to the interaction between piezoelectric and ultrasonic forces (O'Neill and Mudawar, 2020; Turkyilmazoglu and Alofi, 2024; Zheng et al., 2024). Analyzing the PU-AP hydrodynamic model reveals that the fluid flow inside the micro-tapered hole exhibits cyclonic flow and experiences substantial fluctuations in pressure gradient. The k-ε turbulence model, when applied to the analysis of large time-averaged strains, meets Reynolds stress constraints; therefore, with this model, we can ensure that the flow accurately adheres to the fundamental laws of turbulence. Furthermore, the model integrates curvature- and vorticity-related terms into the turbulent viscosity calculation, with adjustments to the dissipation rate equation based on the vorticity fluctuation equation. This enhancement enables the model to more precisely capture the physical dynamics of cyclic expansion and contraction during the micro-tapered hole polishing process, particularly in the context of rotating flow fields, boundary layers, and flow separation. Consequently, the k-ε model is well-suited for describing the turbulent kinetic energy of abrasive flows (Li et al., 2017; Wu et al., 2024a). Its formulation is as follows:

$$\frac{\partial(\rho k)}{\partial t}+\frac{\partial(\rho k\boldsymbol{v})}{\partial x_i}=\frac{\partial}{\partial x_j}\left[\left(\mu+\frac{\mu_{\mathrm{t}}}{\sigma_k}\right)\frac{\partial k}{\partial x_j}\right]+G_{\mathrm{b}}+G_{\mathrm{k}}-\rho\varepsilon+Y_{\mathrm{M}}, \tag{1}$$

$$\frac{\partial(\rho\varepsilon)}{\partial t}+\frac{\partial(\rho\varepsilon\boldsymbol{v})}{\partial x_i}=\frac{\partial}{\partial x_i}\left[\left(\mu+\frac{\mu_{\mathrm{t}}}{\sigma_\varepsilon}\right)\frac{\partial\varepsilon}{\partial x_j}\right]+\rho C_1E\varepsilon-\rho C_2\frac{\varepsilon^2}{k+\sqrt{\nu\varepsilon}}, \tag{2}$$

where ρ is the fluid density, k is the turbulent kinetic energy, t is the time variable, $\boldsymbol{v}$ is the fluid velocity, x_i and x_j are the coordinate components, μ is the molecular viscosity, μ_{t} is the turbulent viscosity coefficient, ε is the dissipation rate, σ_k and σ_ε are the Planck's numbers of k and ε, respectively, G_{b} is the buoyancy-induced turbulent kinetic energy, G_{k} is the turbulent kinetic energy due to the mean velocity gradient, Y_{M} is the pulsating expansion terms in compressible turbulence, E is the fluid strain, and ν is the kinematic viscosity. Other empirical parameters are as follows: $C_1=\max\left(0.43,\ \frac{\eta}{\eta+5}\right)$, $C_2=1.9$, $\sigma_k=1.0$, $\sigma_\varepsilon=1.2$, $\eta=\sqrt{(2E_{ij}\cdot E_{ij})}\,\frac{k}{\varepsilon}$ is an intermediate variable, E_{ij} is the velocity strain rate along the x_{ij}-direction, $\mu_{\mathrm{t}}=\rho C_\mu k^2/\varepsilon$, and C_μ is the empirical constant. This model is able to adequately characterize the various flow features inside the boundary layer as a function of velocity, mean strain, coordinate rotational velocity, angular velocity, and turbulence parameters. Considering the features described above, the k-ε model has great advantages in describing the flow field of jets, boundary layer fluids, and wall shear flows. The micro-tapered hole fluid domain needs to satisfy a continuity condition where variables such as fluid velocity, pressure, and density are quantities that are locally averaged in each grid cell. Assuming that the polished fluid is inviscid and incompressible, the continuity equation and momentum of each mesh can be described as (Xu P et al., 2025; Zhang et al., 2025; Zheng et al., 2025b):

$$\nabla\cdot\boldsymbol{v}=0, \tag{3}$$

$$\rho\frac{\partial\boldsymbol{v}}{\partial t}+\rho(\boldsymbol{v}\cdot\nabla)\boldsymbol{v}=-\nabla P+\nabla\cdot[\mu(\nabla\boldsymbol{v}+\nabla\boldsymbol{v}^{\mathrm{T}})]+\rho\boldsymbol{g}+\boldsymbol{F}, \tag{4}$$

where P is the fluid pressure, $\boldsymbol{g}$ is the gravitational acceleration, $\boldsymbol{F}$ is the average interaction force exerted on the fluid by the particles in the mesh, and ∇ is the Hamiltonian operator.

2.2 Discrete unit model for the PU-AP model (DPM)

The micro-tapered hole polishing procedure utilizes high-frequency random impacts between abrasive grains and the wall surface to effectively remove material from the subject. The key to understanding the polishing impact of PU-AP lies in analyzing the motion pattern of abrasive grains and the characteristics of their collisions with the wall; this can be done by employing flow field parameters. We employ the enhanced

wall treatment (EWT) method due to the crucial role of the near-wall flow in determining the impact velocity of the abrasive grains (Sheikholeslami et al., 2018; Li et al., 2023b; Zheng et al., 2024). The significant disparity in the sizes of the inlet and outlet diameters of the micro-tapered holes, approximately tenfold, results in the accumulation of abrasive particles and subsequent blockage of the flow channel. Consequently, it is imperative to maintain an abrasive particle volume fraction of less than 10%. In contrast to previous models for multiphase flow, the DPM has the capability to accurately depict the path of each abrasive grain. The equation governing the path of abrasive particles from injection to escape can be expressed using Newton's second law:

$$m_a\frac{\mathrm{d}\boldsymbol{v}_a}{\mathrm{d}t}=m_a\frac{18\mu}{\rho_a d_p^2}\frac{C_D Re_p(\boldsymbol{v}-\boldsymbol{v}_a)}{24}+m_a\frac{\boldsymbol{g}(\rho_a-\rho)}{\rho_a}+\frac{m_a\rho}{2\rho_a}\frac{\mathrm{d}(\boldsymbol{v}-\boldsymbol{v}_a)}{\mathrm{d}t}+\frac{5.188m_a\rho\sqrt{\nu}\,\boldsymbol{d}_{ij}(\boldsymbol{v}-\boldsymbol{v}_a)}{\rho_a d_p(\boldsymbol{d}_{lk}\boldsymbol{d}_{kl})^{\frac{1}{4}}},\tag{5}$$

where m_a, $\boldsymbol{v}_a$, ρ_a, and d_p are the mass of the abrasive grain, velocity of the abrasive grain, density of the abrasive grain, and diameter of the abrasive grain, respectively. C_D is the drag coefficient, $Re_p=|\boldsymbol{v}-\boldsymbol{v}_a|d_p/\nu$ is the grain-equivalent Reynolds number, and $\boldsymbol{d}_{ij}$ is the deformation tensor. The first term is the drag force, the second term is the gravitational force, the third term is the virtual mass force, and the last term is the Saffman lift force. Also, due to the low concentration of abrasive grains, the instantaneous fluctuation velocity of the abrasive grain trajectory can be solved by the discrete random wave (DRW) model (Mofakham and Ahmadi, 2020; Yin et al., 2020; Wang CY et al., 2025).

Due to the inelastic nature of the collisions, a portion of the kinetic energy of the abrasive particles is used up when they bounce back from the wall. This might result in unpredictable alterations to the path of the particles. To accurately predict the overall path of the abrasive particles, a coefficient of recovery is established by considering the ratio of the particle's rebound velocity to its initial velocity, as depicted in Fig. 2. The coefficient of recovery is determined by the material qualities of the rebound wall and the angle of incidence of the particle, α. The energy dissipation of abrasive grain–wall collisions in the PU-AP process

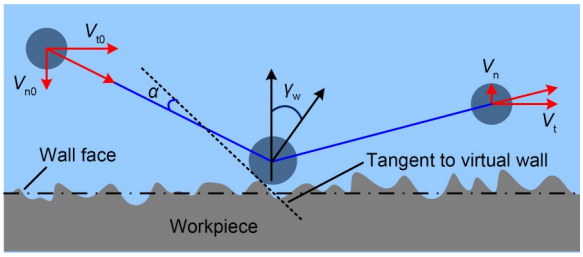

Fig. 2 Abrasive grain–wall impact erosion process. γ_w is the normal deflection angle of the contact between the particle and the rough wall surface

for SUS316L stainless steel can be solved using the commonly used coefficient of recovery model (Grant and Tabakoff, 1975; Forder et al., 1998; Li et al., 2025a). This model can be expressed as:

$$e_n=\frac{V_n}{V_{n0}}=0.998-0.78\alpha+0.19\alpha^2-0.024\alpha^3+0.027\alpha^4,\tag{6}$$

$$e_t=\frac{V_t}{V_{t0}}=1-0.78\alpha+0.84\alpha^2-0.21\alpha^3+0.028\alpha^4-0.022\alpha^5,\tag{7}$$

where e_n is the normal restitution coefficient, e_t is the tangential restitution coefficient, V_n is the normal velocity after the collision, V_t is the tangential velocity after the collision, V_{n0} is the normal velocity before the collision, V_{t0} is the tangential velocity before the collision, and α is the reflection angle of abrasive grains hitting the surface of the workpiece, which can be used to predict the impact erosion process caused by abrasive grain–wall interactions.

2.3 Abrasive grain–wall erosion model

PU-AP polishing utilizes the high-frequency stochastic impacts of abrasive particles to achieve precise polishing of micro-tapered hole walls. Consequently, it is imperative to develop a corresponding abrasive–wall erosion model to evaluate the erosion efficiency and distribution characteristics of the wall under ultrasonic vibration coupling conditions. In this study, the workpiece material is 316L stainless steel, which exhibits plasticity, and the abrasive particles we employ are angular-shaped. The Finnie model is predominantly applicable to plastic materials and provides comprehensive predictions of material removal mass based on the number of abrasive impacts, the incident velocity of the abrasives, and their incident angle relative

to the material surface (Finnie, 1960, 1972; Tarodiya and Levy, 2021). The advantages of the Finnie micro-cutting model in analyzing material cutting wear processes work synergistically with the PU-AP polishing method. Thus, the Finnie micro-cutting model is suitable to act as the abrasive–wall erosion model. The Finnie model can be mathematically represented as:

$$E_r = k_r V_p^2 f(\gamma), \tag{8}$$

where E_r is the erosion wear rate, k_r is a model constant, V_p is the velocity of abrasive grain movement, and $f(\gamma)$ is a dimensionless function of the angle of impact, expressed as:

$$f(\gamma) = \begin{cases} \frac{1}{3}\cos^2\gamma, & \tan\gamma \geqslant \frac{1}{3}, \\ \sin(2\gamma) - 3\sin^2\gamma, & \tan\gamma < \frac{1}{3}, \end{cases} \tag{9}$$

where the amount of surface wear on the micro-tapered holes can be characterized as:

$$m_e = E_r N_p m_p. \tag{10}$$

In Eq. (10), m_p is the mass flow rate of abrasive particles, and N_p is the number of abrasive particles hitting the wall of the micro-tapered hole.

3 PU-AP modeling methodology

3.1 Principle of PU-AP processing

Valveless piezoelectric micropumps induce vibrations in piezoelectric materials by applying an electrical voltage, resulting in minute alterations in pressure (Shan et al., 2022). To achieve a constant flow of fluid, the difference in flow rate between the intake and return flow of the major and minor diameters of the chamber is combined. Hence, we draw inspiration from the operational mechanism of the valveless piezoelectric micropump and propose a micro-tapered hole cleaning technique using PU-AP. Fig. 3a illustrates the components of the PU-AP polishing system, which primarily include piezoelectric ceramics, a transformer, an inverter, a power supply, centrifugal stirring paddles, stirring paddles, and a micro-tapered hole workpiece. The piezoelectric ceramics are firmly attached to the upper wall of the workpiece and induce high-frequency vibrations in the micro-conical perforations. The inner cavity of the micro-tapered hole undergoes periodic variations in volume. The robust interconnection between the micro-cone surface and the abrasive grain flow results in the formation of intermittent jets within the flow field through the micro-tapered hole. The maximum expansion of the micro-tapered hole results in a significant water hammer effect. Simultaneously, the abrasive particles penetrate the fluid boundary layer as a result of the disparity in inertia between the abrasive particles and the fluid. The turbulent and high-frequency collisions with the rough wall surface significantly improve the efficiency and effectiveness of the polishing process, as shown in Fig. 3b. Transformers and frequency converters are employed in this procedure to control the amplitude and vibrational frequency in the piezoelectric ceramics. The uninterrupted path of the abrasive particles and the fluid flow enables dynamic control of the polishing location and effectiveness.

The primary benefits of this PU-AP polishing system are: (1) Piezoelectric ceramics are used to achieve high-frequency periodic changes in the volume of the inner cavity of the micro-tapered hole. This overcomes the limitation of the natural infiltration diameter of the fluid and enables efficient polishing of micro- and nano-scale flow paths. (2) By adjusting the vibrational amplitude and frequency of the piezoelectric ceramics, focused polishing of a specific area can be achieved. This improves the uniformity of surface roughness on the inner wall of the micro-tapered hole. Additionally, the high turbulence of the internal flow field reduces the occurrence of wall scratches and damage. (3) The forceful collisions of abrasive particles against the wall surface, as caused by the water hammer effect and wall shrinking, will enhance the rate of polishing.

The PU-AP micro-tapered hole polishing process achieves precise polishing at a micrometer to nanometer scale by using high-frequency collisions between abrasive grains and the inner wall surface, resulting in micro-cutting of the wall surface material. Fig. 3c illustrates the process, where material is removed during each vibrational cycle of a micro-tapered hole. During the initial vibration stage, a tiny quantity of inert abrasive particles can be found at the bottom of the micro-tapered hole. This is caused by infiltration of the abrasive flow and the isobaric surface effect.

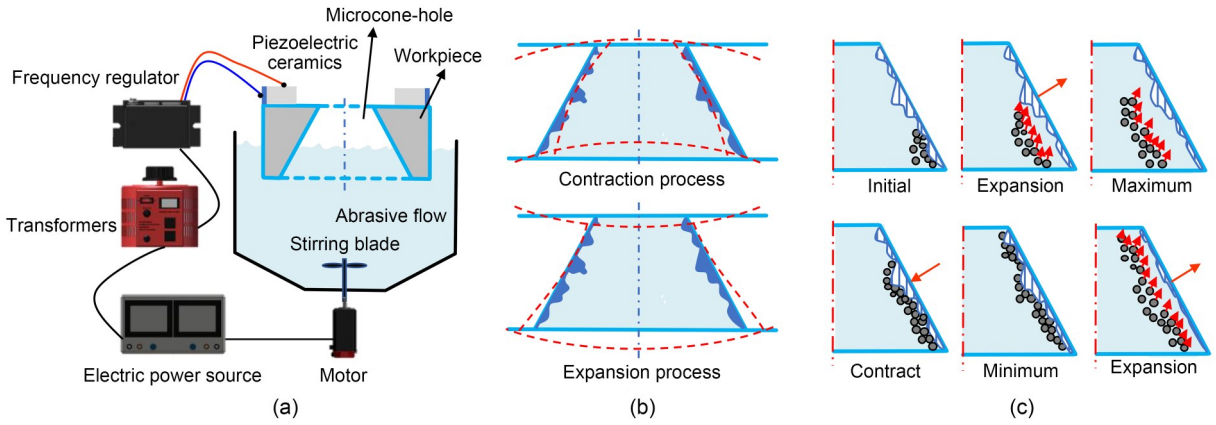

Fig. 3 PU-AP polishing principle: (a) schematic diagram; (b) asymptotic expansion–contraction process; (c) abrasive grain movement trajectory

As the wall expands, the fluid and abrasive particles tend to collide heading towards the wall, due to the differential pressure effect. However, the varying mass forces between the liquid and the abrasive particles result in distinct movement inclinations. At the point where the volume of the micro-tapered hole cavity is at its highest, the distance between the abrasive particle and the wall surface is also at a maximum. The direction of the wall contraction is determined by the direction of abrasive particle migration, leading to the most substantial impact force. The effect of the abrasive wall can be separated into two components: a perpendicular component and a parallel component, which enhance each other. The vertical force component can potentially inflict damage to the wall material and diminish its adherence. On the other hand, the parallel component can result in a micro-cutting impact on the micro-peaks of the micro-tapered hole's wall surface. During the contraction process, the abrasive particles undergo lateral movement along the wall surface of the micro-tapered hole due to the influence of fluid. Meanwhile, because of the strong parallel component of the impact force, the abrasive grains will be expelled from the flow field along with the leftover material from cutting.

3.2 Numerical model and boundary conditions

The expansion and contraction process of the workpiece, which is caused by the reverse piezoelectric effect of the piezoelectric module, is illustrated in Figs. 4a and 4b. The restricting flow field refers to the space between the micro-tapered holes. Prior to entering the restricted flow area, it is important to ensure that the abrasive stream possesses adequate turbulent kinetic energy and that the abrasive particles are evenly dispersed within the fluid. This is necessary to achieve uniform polishing on the surface of the workpiece. With this in mind, we create a numerical model to simulate the PU-AP polishing procedure for the machining of micro-tapered holes. The sidewall surfaces of the micro-tapered holes in the flow field are designed to simulate dynamic layers. These layers are either added or removed based on the height of the grid layer at the near-wall boundary. Based on the piezoelectric ceramic ultrasonic vibration generation mode, the vibrational displacement of the inner wall surface follows a sinusoidal pattern. The frequency converter and transformer are used in concert to adjust the wall's vibration parameters, as illustrated in Fig. 3b. The abrasive flow is considered to be the flow of an incompressible and non-viscous fluid.

The geometric characteristics and boundary conditions of the flow field inside the micro-tapered hole are shown in Table 1. The main phase is composed of liquid water, while the secondary phase consists of a 7% volume fraction of silica (SiO_2) abrasive. Table 2 displays the specific characteristics of the fluid medium. In order to decrease the computational complexity, the energy equation is omitted, and the inner wall surface of the micro-tapered hole is considered as an adiabatic rigid body. Ultrasonic shaking of the wall induces pressure variations in the restricted flow field, resulting in highly nonlinear characteristics. To prevent significant changes in fluid pressure, the pressure staggering option (PRESTO!) (Li et al., 2023c, 2023d; Zheng et al., 2023a, 2023b) scheme utilizes a

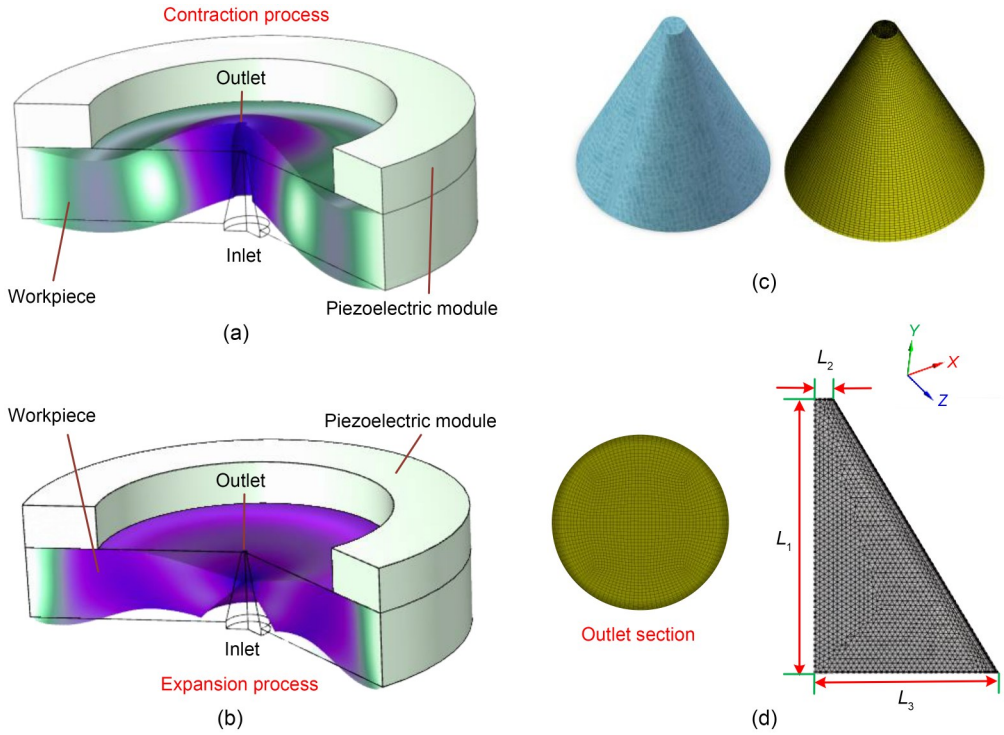

Fig. 4 Geometric model and constrained flow field for the PU-AP polishing method: (a) contraction process; (b) expansion process; (c) overall morphology of the micro-tapered hole and the meshing configuration; (d) outlet section and the grid cross-sectional view of micro-tapered hole. L_1: height; L_2: outlet radius; L_3: inlet radius

Table 1 Geometric parameters and boundary conditions of the constraint module

Item	Description
Inlet	Velocity-inlet boundary conditions
Outlet	Free outflow boundary conditions
Wall	No-slip wall boundary conditions
Zone	SiO_2, water
Ultrasonic frequency, f (kHz)	50, 75, 100, 150
Vibration amplitude (μm)	1.95, 2.44, 3.05, 3.81
Workpiece	SUS316L
Height, L_1 (μm)	30
Outlet radius, L_2 (μm)	2
Inlet radius, L_3 (μm)	15
Reference pressure (Pa)	1.01×10^5

Table 2 Physical parameters for the abrasive flow

Parameter	Value
Water density (kg/m^3)	998
Water viscosity (Pa·s)	0.00103
SiO_2 density (kg/m^3)	2200
SiO_2 diameter (μm)	0.06
SiO_2 volume fraction (%)	7
Inlet velocity (m/s)	1×10^{-6}
Hydraulic diameter (μm)	5.13
Main channel turbulence intensity (%)	5
Gravity acceleration (m/s^2)	9.81

preloaded staggered pattern. Furthermore, a semi-implicit method is employed to solve the interconnected pressure–velocity problem by considering the pressure–link equation. The momentum, turbulent kinetic energy, and turbulent dissipation rate are discretized using a windward format with second-order accuracy.

An appropriate meshing strategy is critical for achieving stability and accuracy of numerical simulations (Li QH et al., 2024; Wang T et al., 2025). The overall morphology of the micro-tapered hole and the meshing configuration are shown in Fig. 4c, with a hexahedral mesh employed for the flow field within the micro-tapered hole. Given the importance of the flow field's distribution characteristics and the abrasive particle trajectories, a sufficiently refined boundary layer mesh near the wall region is imperative (Li et al., 2025b; Zheng et al., 2025a). To enhance observability, a specific cross-section was selected for examination, as illustrated in Fig. 4d. Moreover, to ensure

that both discretization errors and rounding errors remained low, and to meet the accuracy and reproducibility requirements of the simulation results, a mesh independence study was conducted as depicted in Fig. 5. This study revealed that the pressure and time simulation results across five different mesh quantities exhibited similar trends, with the sampling curves for N= 298690 and 382399 showing particularly strong agreement in the negative pressure trend. However, at lower mesh densities (N=111964, 167962, and 208185), the sampling curves diverge in terms of negative pressure. To ensure the accuracy of the numerical simulation results and to strike a balance between computational precision and time efficiency, a mesh count of 298690 was chosen.

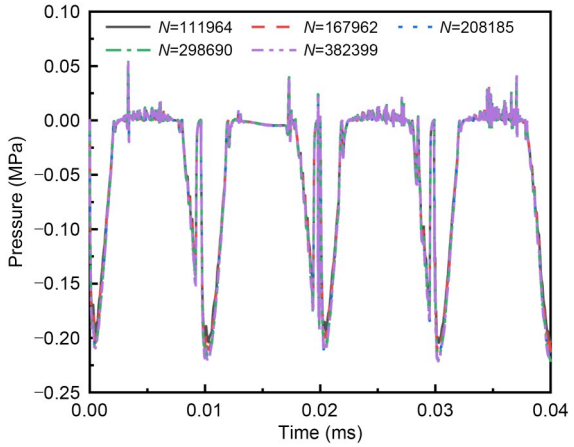

Fig. 5 Grid-unrelated validation (pressure–time distribution plots at multiple points)

4 Numerical simulation results

4.1 Evolutionary mechanism of PU-AP expansion and contraction

During the expansion and contraction of the PU-AP, the rapid fluctuations in the volume of the internal flow field result in elevated pressure and turbulent features. In order to predict the wall polishing effects, it is essential to examine the flow field characteristics of the inner wall surface. Fig. 6a displays the pressure distribution on the inner wall surface during the expansion and contraction cycle in a 3D graphic. The flow field within the micro-tapered holes in the circular platform bus demonstrates a consistent change pattern. Near the exit, where the cross-sectional area is small, the deformation amplitude of the workpiece in this region remains relatively stable during the expansion process, leading to a negligible change in internal pressure.

Fig. 6b illustrates the fluctuations in pressure that occur during the expansion and contraction cycles. During each cycle, the overall similarity in the pattern of pressure change can be described by six distinct points. In Fig. 6b, Point 1 marks the initial stage of progressive expansion, characterized by a rapid oscillation and expansion of the volume of the micro-tapered hole. This stage also exhibits the steepest slope of pressure drop. Over time, the micro-tapered hole reaches its maximum volume at Point 2, with the maximum negative pressure inside it being lower than −0.2 MPa. Afterwards, the rate of volume change progressively reduces, and the volume of the micro-tapered hole achieves a state of equilibrium (similar to the initial condition) at Point 3, where the pressure varies slightly around 0 MPa.

At the onset of the contraction phase at Point 4, there is no negative pressure area. Nevertheless, following the start of contraction, the rate of pressure alteration reaches a maximum, and the volume within the micro-tapered hole also attains equilibrium. Currently, the highest value of the maximum positive pressure is around 0.02 MPa, as indicated at Point 5. During the subsequent phase, the micro-tapered holes experience rapid compression, causing the internal pressure to surpass atmospheric pressure and vibrate vigorously, until the micro-tapered holes reach an extreme level of compression as indicated at Point 6. Right after this, an analogous cycle of growth and contraction begins. During the expansion and contraction cycle, the negative pressure generated during gradual expansion is greater than the positive pressure generated during gradual contraction. This is because of the varying flow resistance characteristics at the two ends of the micro-tapered hole. This leads to a one-way pumping effect inside the micro-tapered hole, allowing for the creation of controlled fluid flow in a specific direction. This flow acts as a driving force for the polishing of the inner wall of the micro-tapered hole.

In order to analyze the flow field features within the micro-tapered hole during expansion and contraction cycles, we conducted separate studies on the flow pattern alterations at six distinct sites. Observing the changes in the flow field inside the micro-tapered hole

from the cloud diagrams is challenging, since the workpiece wall deformation is small.

At Point 1, the fluid within the conical cavity moves along the flow lines, flowing from the wider opening to the narrower opening. As the fluid reaches the constricted opening, the pressure diminishes as the velocity of flow intensifies, as shown in Fig. 7a. Due to the significant rise in negative pressure within the micro-tapered hole during asymptotic expansion, the fluid is swiftly drawn in from both sides of the hole. At Point 2, the negative pressure at the wider opening of the micro-tapered hole is higher than at the narrower

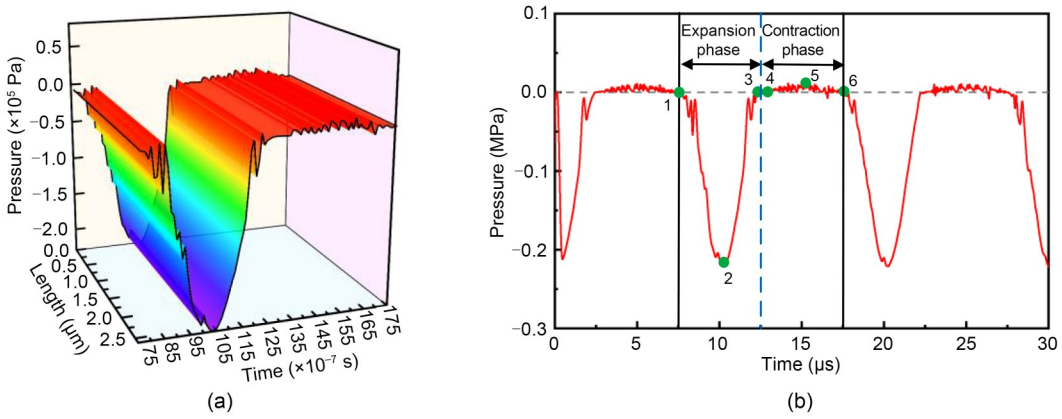

Fig. 6 Cyclical pressure variation curve on the wall surface of a micro-tapered hole: (a) first-cycle time–length–pressure 3D curve; (b) intermediate characteristic point pressure change rule

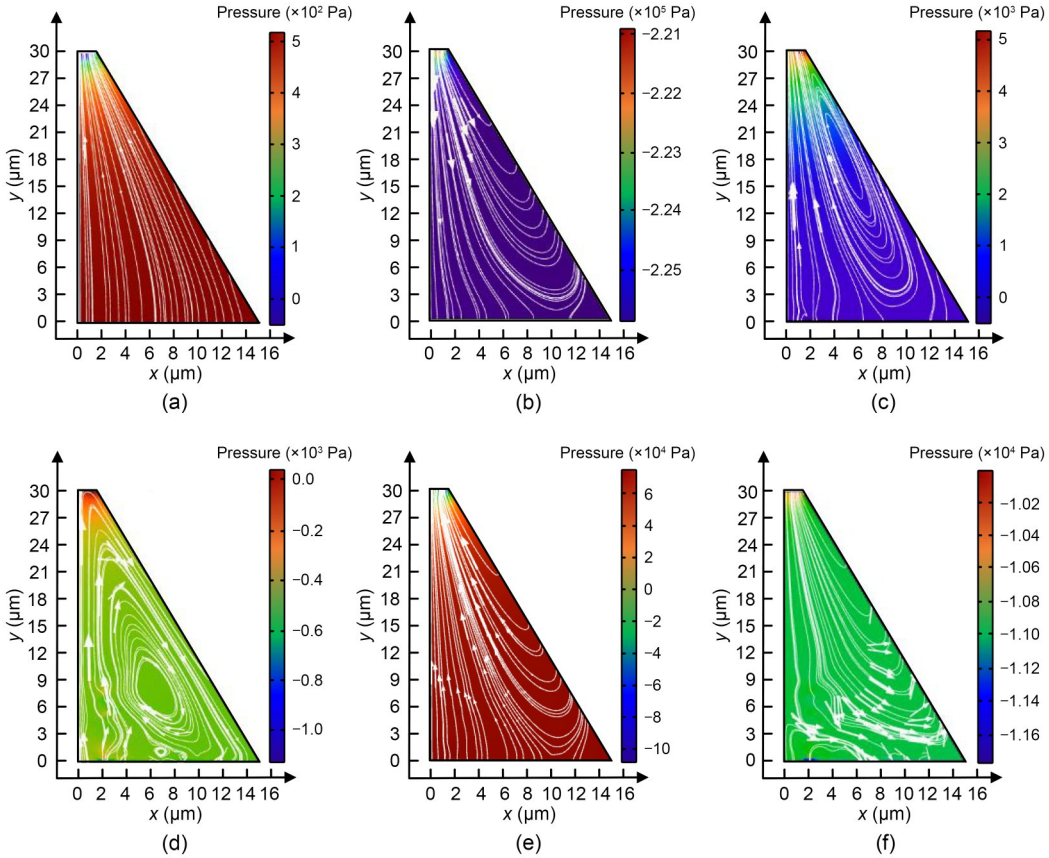

Fig. 7 Changes of flow field pressure and streamline patterns during the cycle: (a) Point 1; (b) Point 2; (c) Point 3; (d) Point 4; (e) Point 5; (f) Point 6. References to color refer to the online version of this figure

opening, with the negative pressure near the wall slightly surpassing that near the center. This results in the fluid within the hole beginning a rotational flow, as shown in Fig. 7b. At this point, the micro-tapered hole experiences a pressure difference of over 0.2 MPa and a velocity difference of 0.1 m/s. Following the slow expansion phase, the pressure in the micro-tapered hole at Point 3 increases quickly, with the pressure at the narrow opening surpassing that at the large opening. The pressure gradient between these two locations decreases to 0.02 MPa. The presence of vibration and deformation in the micro-tapered hole, along with pressure fluctuations in the fluid flow lines, leads to the formation of a vortex around the narrow opening, as illustrated in Fig. 7c.

At Point 4, the fluid vortex close to the wall becomes significantly stronger because of the consistent pressure variations in the conical hole, as shown in Fig. 7d. During the onset of the tapering phase, following a minor initial fluctuation, the pressure in the tapered bore increases quickly. At Point 5, the pressure at the narrow opening of the micro-tapered hole is lower than at the wide opening, with a maximum pressure difference surpassing 0.06 MPa in the area. This causes the flow lines to extend towards the narrow mouth, resulting in an upward shift of the vortex, as shown in Fig. 7e. For the case of Point 6, the pressure increases to 0.02 MPa and then quickly decreases to about 0 MPa, resulting in the formation of a more powerful vortex near the surface of the wall, as depicted in Fig. 7f. At this juncture, one cycle of alterations in the flow field within the conical hole has been completed, and the next cycle starts. During the transition from the expansion peak to the compression peak, namely from Point 2 to Point 5, a Dean vortex can be observed in the inner flow field. The reverse flow of the flow field near the wall efficiently smooths the wall surface.

4.2 Collision process between PU-AP abrasive particles and the wall surface

The angle at which the abrasive grains hit the wall and the speed at which they move in the flow field are the key factors that affect the achieved level of polishing on the wall. Notably, it is feasible to study the trajectory of the abrasive grains in the flow field throughout their life cycle in order to anticipate the polishing impact. Fig. 8 illustrates the path followed by the abrasive grains within the conical cavity.

During the initial stage, the workpiece wall expands, leading to a noticeable negative pressure along the wall. This negative pressure causes the SiO_2 abrasive grains to be driven into the surface of the workpiece and gather near the intake. The Dean vortex induces intense turbulence and high velocity near the wall, leading to frequent contact between the abrasive particles and the wall. These particles slowly and steadily travel towards the exit. Nevertheless, as the wall begins to move back, the abrasive particles encounter a force that is aligned with and directed upwards along the wall, in accordance with Newton's third law and the principle of force decomposition. This force propels the particles to swiftly escape the flow field. In close proximity to the workpiece wall's departure, there is a notable decrease in both the frequency and length of grain impact, resulting in a major decline in the effectiveness of the polishing. By observing the trajectory of the abrasive grains throughout their lifespan, it becomes evident that the influence of centrifugal force prevents the abrasive grains from entering the Dean vortex. Instead, they remain in the zone close to the wall, hence reducing the energy consumption of the polishing process. To summarize, the workpiece wall at the inlet region exhibits superior polishing, whereas the polishing effect near the outlet experiences a minor decline.

4.3 Effect of vibrational frequency and amplitude on the polished area

A crucial step in predicting the erosional effect on the polishing area is quantitatively analyzing the effects of different frequencies and amplitudes on the flow field pressure changes, as well as the trajectory of abrasive grains in the micro-tapered hole. This can be done based on the principle of piezoelectric ultrasonic coupled abrasive flow material removal. The variations in pressure within the micro-tapered hole exhibit similar patterns at different frequencies and amplitudes. The main differences lie in the maximum and minimum values of the pressure, as discussed in Sections 4.1 and 4.2. Therefore, these differences will not be described again here.

Fig. 9a displays the average and labeled variations in the pressure peaks and valleys of the flow field, obtained by measuring the first 20 cycles of expansion and contraction at different vibrational frequencies. As the ultrasonic frequency increases from 75 to 150 kHz, the negative pressure in the micro-tapered

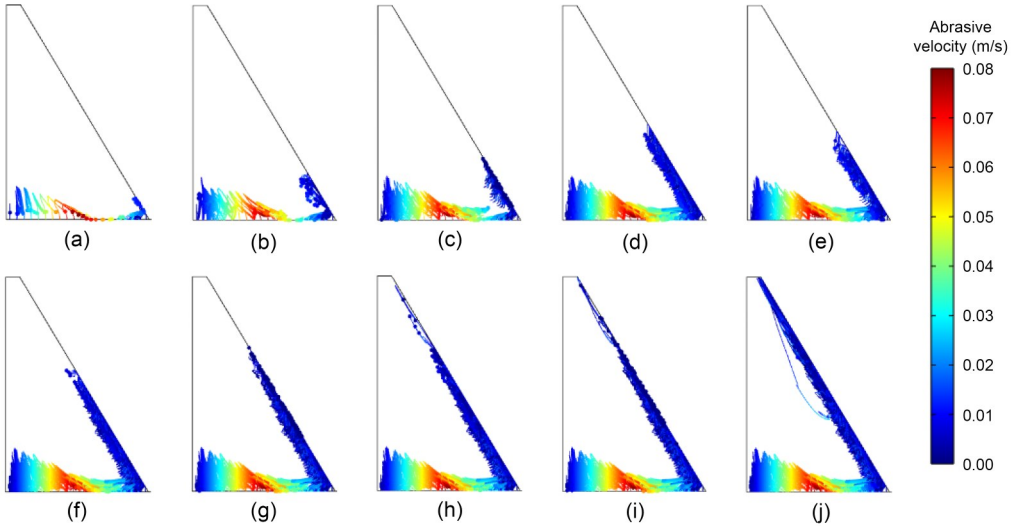

Fig. 8 Trajectory of the abrasive grains: (a) 0.0125 ms; (b) 0.025 ms; (c) 0.05 ms; (d) 0.075 ms; (e) 0.1 ms; (f) 0.125 ms; (g) 0.14 ms; (h) 0.145 ms; (i) 0.15 ms; (j) 0.2 ms. References to color refer to the online version of this figure

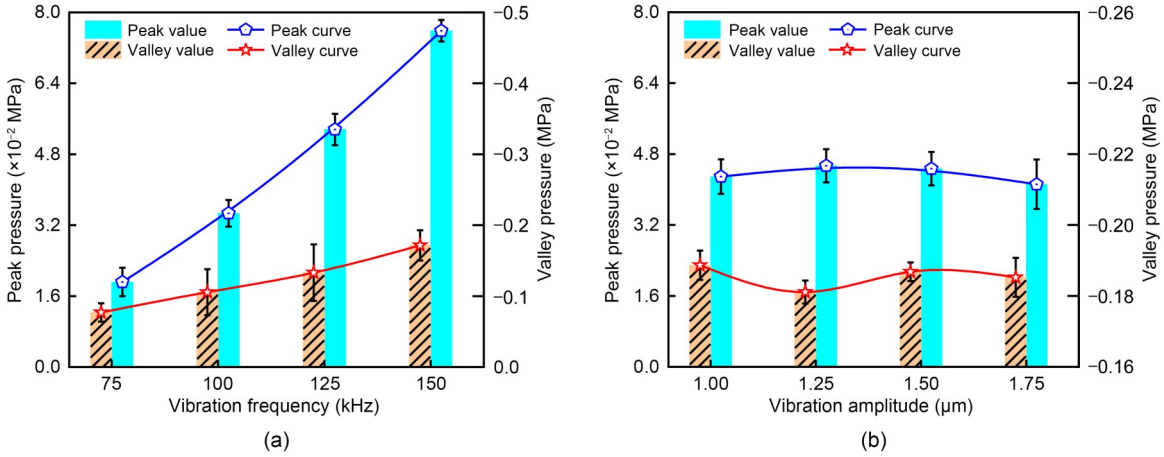

Fig. 9 Plot of vibration frequency, amplitude, and pressure variation: (a) variations of pressure peaks and valleys under different vibration frequencies; (b) variations of pressure peaks and valleys under different vibration amplitudes

hole increases linearly with the positive pressure. Notably, the rate of increase in negative pressure is significantly greater than that of positive pressure.

Figs. 10a1–10a4 illustrate the velocity, trajectory, and effectiveness of abrasive grain movement in eroding walls at a frequency of 75 kHz. At first, the abrasive granules are primarily concentrated in the central area of the conical hole region. The external force generated is insufficient to move the abrasive grains towards the wall due to the small negative pressure near the wall. The grains exhibit downward movement within the hole only as a result of wall expansion, contraction, and inertial forces, without any lateral movement along the wall.

At a frequency of 100 kHz, there is a notable augmentation in both negative and positive pressures within the flow field as compared to 75 kHz, as shown in Figs. 10b1–10b4. The velocity of the abrasive grains near the wall is higher than in other areas. In addition, greater negative pressure, mass force, and Dean vortex centrifugal force propel the abrasive grains, causing them to cover a larger area and increase in intensity, while also pushing the primary polishing region upwards, as depicted in Fig. 10b4. At a frequency of 125 kHz, the alterations are illustrated in Figs. 10c1–10c4. The near-wall abrasive grain motion velocity almost doubles as compared to 75 and 100 kHz. The augmented suction, in conjunction with the pressure

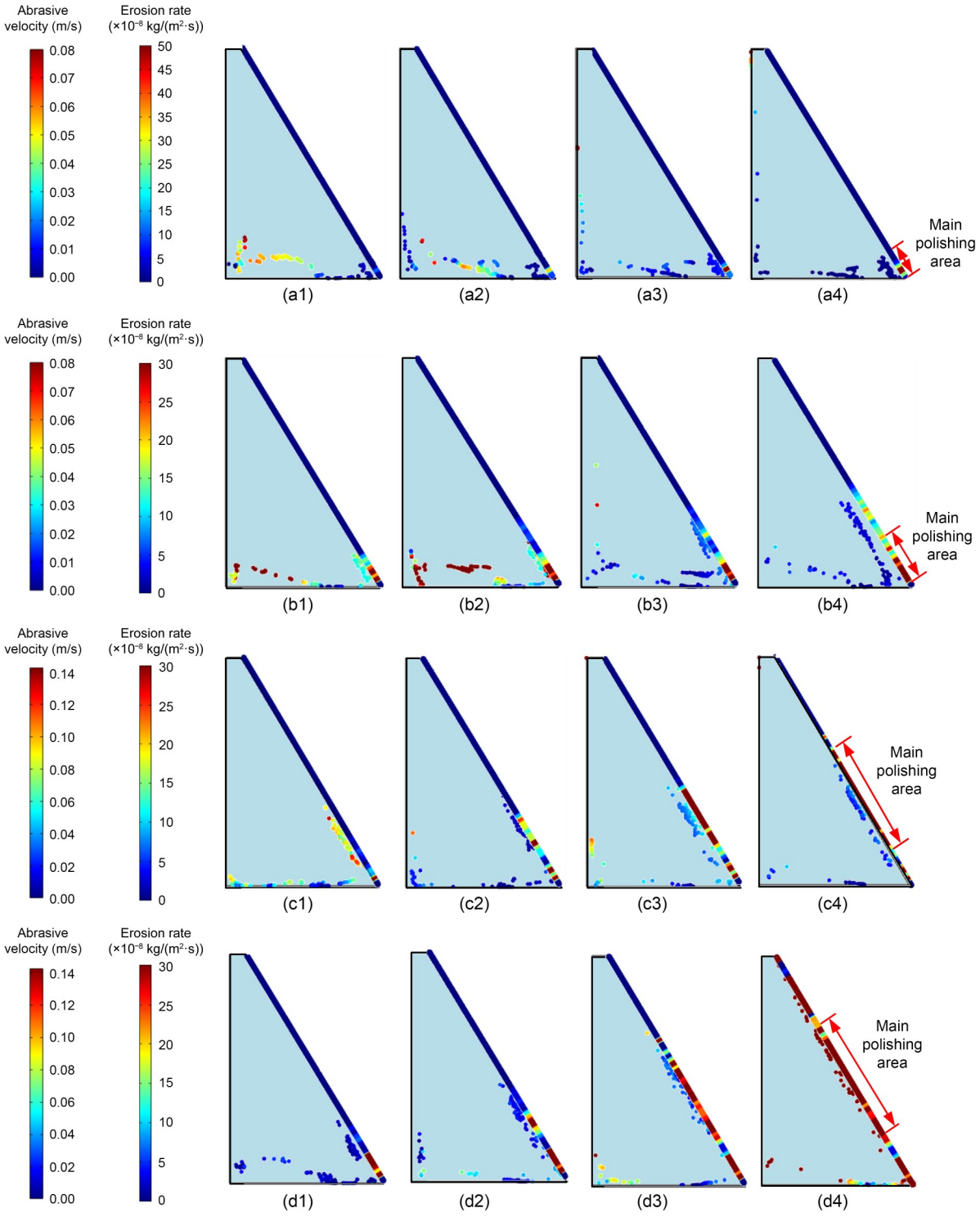

Fig. 10 Effect of vibrational frequency on flow field pressure, abrasive grain trajectory, and key polishing areas: (a1) 75 kHz, 0.025 ms; (a2) 75 kHz, 0.075 ms; (a3) 75 kHz, 0.125 ms; (a4) 75 kHz, 0.15 ms; (b1) 100 kHz, 0.025 ms; (b2) 100 kHz, 0.075 ms; (b3) 100 kHz, 0.125 ms; (b4) 100 kHz, 0.15 ms; (c1) 125 kHz, 0.025 ms; (c2) 125 kHz, 0.075 ms; (c3) 125 kHz, 0.125 ms; (c4) 125 kHz, 0.15 ms; (d1) 150 kHz, 0.025 ms; (d2) 150 kHz, 0.075 ms; (d3) 150 kHz, 0.125 ms; (d4) 150 kHz, 0.15 ms. References to color refer to the online version of this figure

gradient and drag force, results in the abrasive particles predominantly moving alongside the surface, thereby enlarging the erosional region to be several magnitudes greater than that for 100 kHz, and further intensifying the effect. The main area for polishing at this frequency is shown in Fig. 10c4. At a frequency of 150 kHz, there are many similarities in the observed patterns. These include higher speeds of abrasive grain movement along the wall, larger areas of erosion, and greater severity of erosion. These observations are illustrated in Figs. 10d1–10d4.

Overall, the frequency has a substantial impact on both the flow field pressure and the trajectory of the abrasive grains. As the frequency increases, the pressure differential in the flow field also increases because of the varying flow resistance of the conical hole. This, in turn, leads to a higher trailing force on the abrasive grains along the wall surface. In addition, this causes the abrasive granules to migrate in a tangential direction along the surface of the wall. Moreover, the heightened frequency amplifies the Dean vortex within the flow field, intensifying the mass force and centrifugal force exerted on the abrasive particles. This, combined with the traction force of the flow field, propels the abrasive particles to undergo haphazard collisions along the wall, thereby refining the surface of the conical hole.

Fig. 9b illustrates the fluctuation of pressure peaks and valleys at different amplitudes, for a frequency of 100 kHz. As the amplitude increases, the maximum pressure remains relatively constant, and the minimum pressure changes slightly without a clear pattern. While the vibrational frequency of the flow field pressure change and the trajectory of the abrasive grain movement are comparable, the erosion impact of abrasive grains differs depending on the amplitude. Fig. 11 showcases the velocity, path, and effectiveness of abrasive grain movement in relation to wall erosion at various amplitudes.

By examining Fig. 11, it is evident that greater amplitudes lead to increased tangential velocities of abrasive grains near the wall, whereas the erosion rate of the abrasive grains on the wall decreases. As the magnitude of the oscillation grows, the low pressure in the flow field also increases, causing the abrasive particles near the wall to travel more quickly in a tangential direction. However, despite this consistent frequency, the limited number of contacts between the abrasive particles and the wall results in a decrease in the rate of wall erosion. Hence, the key strategy for removing material from the wall in conical holes should be to increase the frequency, in order to maximize the number of contacts between the abrasive grains and the wall in the normal direction. In contrast, the primary strategy for managing the material removal area on the wall is to increase the amplitude, so as to boost the negative pressure.

In order to validate this analysis, we next perform an experimental verification considering the effects of both frequency and erosion rate, using data obtained from simulations and quantitative analysis. These experiments were conducted with a frequency of 100 kHz and an amplitude of 2.44 μm.

5 Construction of the PU-AP experimental platform

In order to determine the effectiveness and superiority of the PU-AP method in polishing the inner walls of micro-tapered holes, it is necessary to build a dedicated experimental platform for conducting polishing trials on the workpiece surface. Due to the extremely small size of the micro-tapered holes, current equipment is insufficient for conducting a thorough structural examination. Hence, it is imperative to analyze the surface morphology and roughness of the micro-tapered holes, scrutinizing each layer individually. We will analyze the surface roughness of the inner walls of the micro-tapered holes using different polishing durations. Our objective is to look for a correlation between polishing duration and polishing effect by comparing these results with those of numerical simulations. This will provide a scientific foundation for future applications.

5.1 Experimental setup assembly

A PU-AP experimental platform was built to assess the morphology of the inner wall surface of micro-tapered holes and to quantitatively characterize their surface roughness, as depicted in Fig. 12. This assembly is comprised of an ultrasonic oscillator, piezoelectric ceramics, a power source, centrifugal stirring paddles, auxiliary stirring paddles, a micro-tapered hole specimen, and a peristaltic pump with a variable flow rate ranging from 2 to 125 mL/min. The abrasive flow

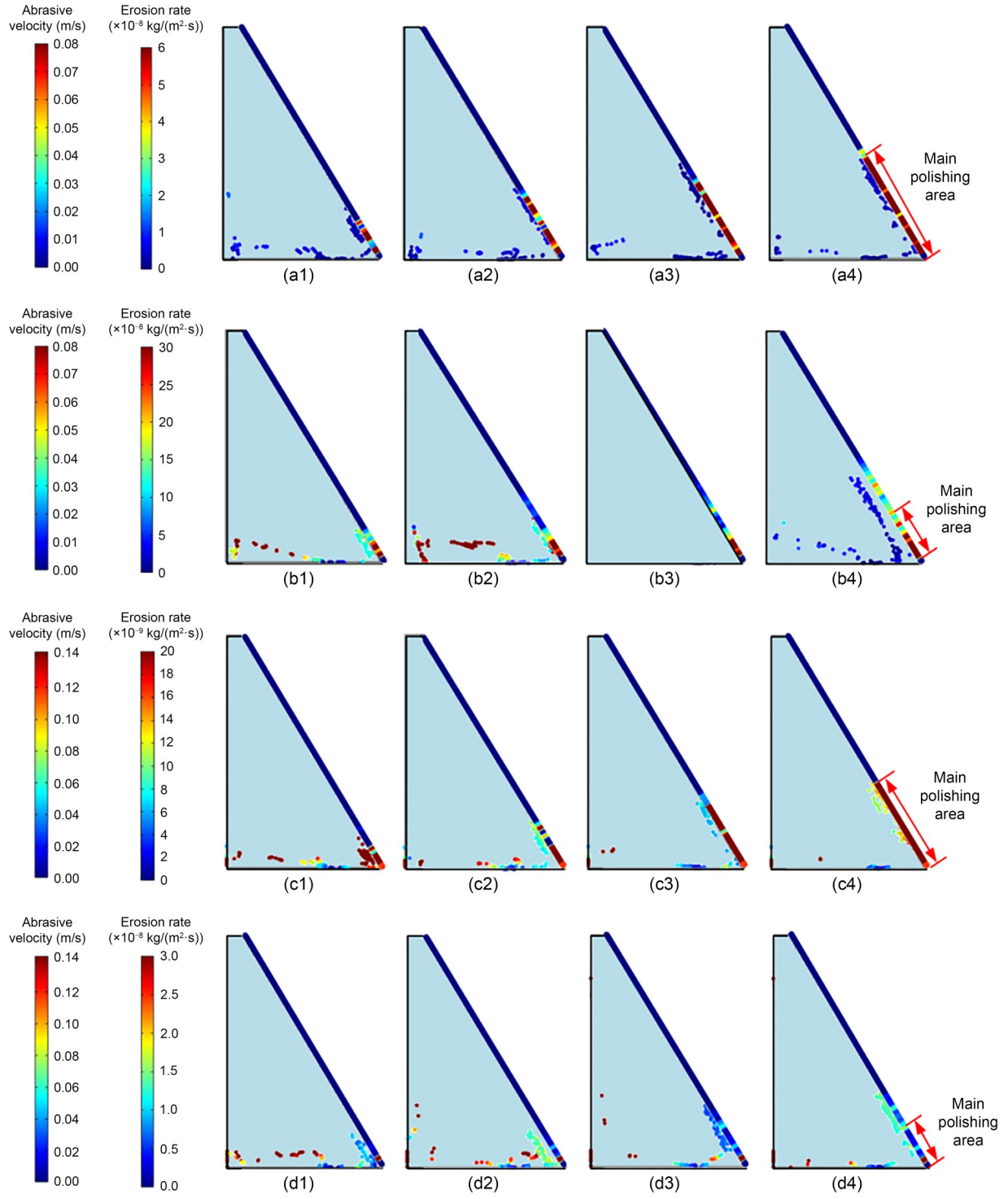

Fig. 11 Effect of vibrational amplitude on flow field pressure, abrasive grain trajectory, and key polishing areas: (a1) 1.95 μm, 0.025 ms; (a2) 1.95 μm, 0.075 ms; (a3) 1.95 μm, 0.125 ms; (a4) 1.95 μm, 0.15 ms; (b1) 2.44 μm, 0.025 ms; (b2) 2.44 μm, 0.075 ms; (b3) 2.44 μm, 0.125 ms; (b4) 2.44 μm, 0.15 ms; (c1) 3.05 μm, 0.025 ms; (c2) 3.05 μm, 0.075 ms; (c3) 3.05 μm, 0.125 ms; (c4) 3.05 μm, 0.15 ms; (d1) 3.81 μm, 0.025 ms; (d2) 3.81 μm, 0.075 ms; (d3) 3.81 μm, 0.125 ms; (d4) 3.81 μm, 0.15 ms. References to color refer to the online version of this figure

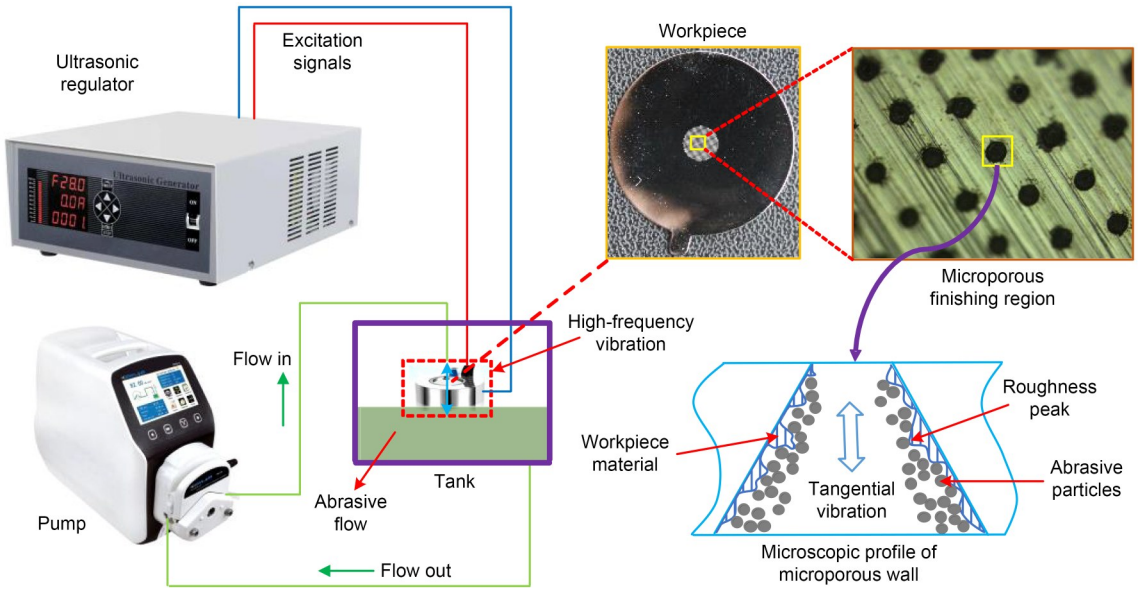

Fig. 12 Experimental workflow

comprises SiO_2 particles, water, and an electrostatic dispersant, with the SiO_2 particles having an average diameter of 0.6 μm and being present at a mass fraction of 7%. A particle concentration that is too high may cause clogging in narrow regions, thereby hindering the polishing process. Conversely, a particle concentration that is too low may fail to provide a strong enough impact on the wall surface, thus markedly diminishing the polishing efficiency. Thus, we use a moderate value of 7%. The sample is composed of 316L stainless steel.

Prior to the polishing procedure, the stirrer evenly distributes the abrasive particles across the abrasive flow by dispersion. The peristaltic pump moves the abrasive stream, which is then recirculated through the vessel and over the specimen. The higher density of the ablated material, in comparison to the SiO_2 abrasive and liquid water, guarantees that the ablated material is primarily deposited toward the bottom of the vessel. This deposition, in addition to frequent cleaning of the vessel, reduces the negative effects of the removed material on the structural surface integrity.

5.2 Polishing experiment results

Surface roughness is a crucial parameter used to assess the surface quality of micro-tapered holes. The microstructural morphology of the hole wall was analyzed using a 3D measuring laser microscope OLS5000 (OLYMPUS, Japan), as shown in Fig. 13. The machining process and the accompanying high temperatures during the creation of micro-tapered holes can lead to an uneven surface and significant debris, which can greatly reduce the quality of these holes.

After undergoing a 4-h PU-AP polishing procedure, a significant decrease in both debris and surface imperfections was detected on the inner wall surface of the micro-tapered holes. The existence of reflective regions in specific areas supports the effectiveness of the proposed PU-AP polishing method in dealing with polishing difficulties related to the inner wall surface of micro-tapered holes. Following a 15-h polishing process, the surface dirt on the inner wall was almost completely eliminated, resulting in an even surface. Nevertheless, this approach fails to offer a quantitative assessment of the effectiveness of the PU-AP polishing procedure. Hence, it is crucial to capture the 3D shape of the inner wall surface of the micro-tapered hole. The small size of the micro-tapered holes and their variations in height make it difficult for the measuring laser microscope to accurately capture their 3D shape. Furthermore, in order to determine the precise surface roughness, it is essential to calculate the difference between the actual height and the target height of the wall.

To facilitate visual examination and comparisons, surface roughness measurements were obtained from both the left and right sides of the micro-tapered hole. The results of the measurements taken at specific

points are shown in Fig. 14. The random and unpredictable nature of the abrasive flow's effect on the structural surface, along with the limitations imposed by the micro-tapered hole, makes it impossible to ensure a consistent surface quality at every point. This results in random fluctuations in the roughness value of the polished area. The surface roughness on the outside edge area of the micro-tapered hole is notably low (i.e., it is smooth) due to the concentrated collision area and high impact intensity of the abrasive grains in this region. As the measuring area moves closer to the inner edge of the micro-tapered hole, there is a gradual increase in surface roughness and a growing fluctuation, which matches the findings obtained from simulations. However, the initial roughness of the machined micro-tapered hole also plays a crucial role in the polishing result. This is because the inner edge region experiences fewer and less intense impacts from abrasive grains, and the original surface roughness has a larger impact on this area.

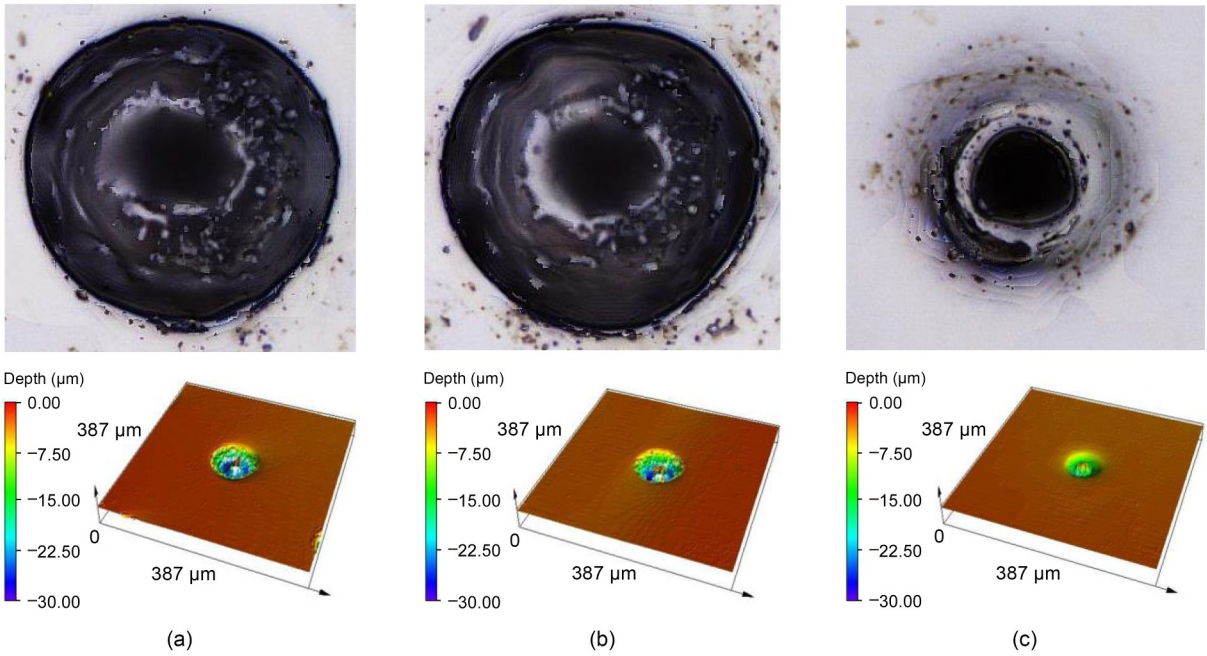

Fig. 13 Surface morphology of micro-tapered holes at different polishing moments: (a) unpolished; (b) after 4 h of polishing; (c) after 15 h of polishing. References to color refer to the online version of this figure

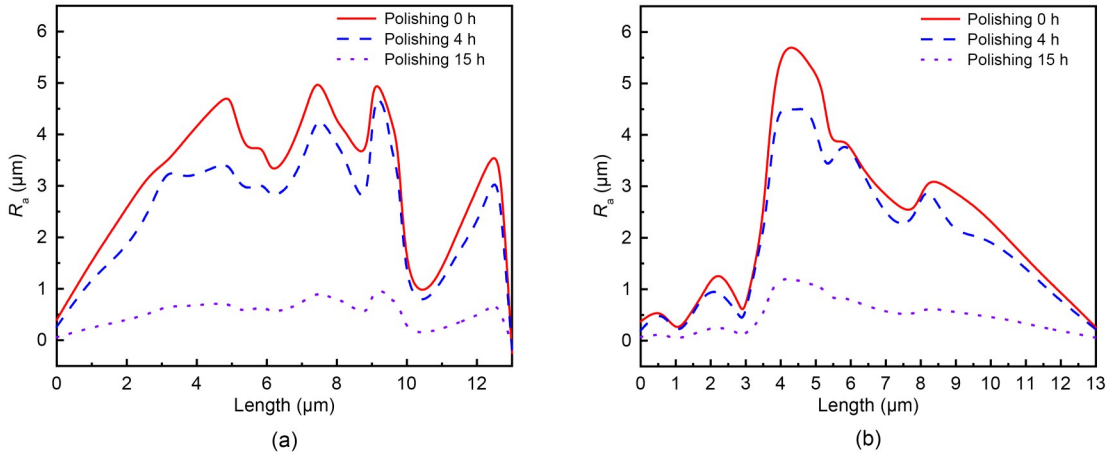

Fig. 14 Surface roughness (R_a) at different polishing moments: (a) left side; (b) right side

6 Conclusions

A novel method was proposed to enhance the effectiveness and efficiency of polishing micro-tapered hole flow channels in microfluidic chips. This method utilizes piezoelectric ultrasound coupled abrasive flow in conjunction with the operational principle of a valveless piezoelectric micropump to actively remove material from the channels. This technique uses the ultrasonic pulse properties of piezoelectric ceramics along with the internal cavitation effect. It overcomes the inherent limitation of fluid infiltration diameter and enables the abrasive particles and fluid to impact the wall surface of the micro-tapered holes at a specific velocity. Consequently, it enhances the efficiency of the AJP method.

The complete calculation of vortex formation, movement of abrasive grains, and erosion of the wall during PU-AP was performed. The rapid fluctuations in the volume of the internal flow field caused by the expansion and contraction of the micro-tapered pores resulted in elevated pressure and turbulent features. Simultaneously, the internal flow field exhibited Dean vortices, which generate centrifugal force that leads to numerous collisions of abrasive particles with the wall and progressive movement towards the outlet at a reduced pace.

The repeated and chaotic collisions of abrasive particles against the surfaces of small, gradually-narrowing holes can enhance the effectiveness and consistency of the polishing process. The polishing effect in specific sections of the micro-tapered holes is determined by the frequency and amplitude of the vibration of the piezoelectric ceramics. The frequency of ultrasonic vibrations has a direct relationship with the presence of valleys and peaks within the cavity. As the vibrational frequency increases, the extent and size of the wall erosion also rise. The polishing position gradually shifts from the wider opening to the narrower opening. The erosion and vibrational amplitude are nonlinearly correlated, mirroring the pattern observed in the pressure valleys and peaks within the micro-tapered hole. Therefore, when deciding upon parameters, it is necessary to account for the vibrational frequency and vibrational amplitude of the piezoelectric ceramics, along with the volume of the inner cavity of the micro-tapered hole.

A PU-AP polishing system was created to thoroughly assess the impact of polishing micro-tapered holes with varying durations of polishing. Measurements from the 3D measuring laser microscope OLS5000 demonstrated that the PU-AP approach effectively eliminates dirt and surface protrusions from the inner wall surface of the micro-tapered holes after 4 h of polishing, resulting in reflections in certain locations. After 15 h, the surface roughness of the micro-tapered hole can be reduced to below 1 μm, and the surface uniformity of the hole wall was high.

The wall quality of micro-tapered holes is important for the development of microfluidic technology. The primary objective of this study was to incorporate ultrasonic vibration into the polishing of wall surfaces in micro-tapered holes. Additionally, we aimed to uncover the phenomena of vortex formation, movement of abrasive grains, and erosion of the wall in conical hole cavities during the process of ultrasonic vibration coupling. Ultimately, utilizing the ultrasonic frequency and amplitude in the design allows for active control of the polishing area. However, PU-AP polishing techniques can still encounter difficulties in terms of material removal and vibrational fatigue effects; the material removal functionality could potentially be improved by pulsation and cavitation. These matters will be investigated in subsequent research.

Acknowledgments

This work is supported by the National Natural Science Foundation of China (Nos. U25A20294, 52175124, 52575546, and 52305139), the Zhejiang Provincial Natural Science Foundation of China (Nos. LQ23E050017 and LZ21E050003), the Fundamental Research Funds for the Provincial Universities of Zhejiang, China (No. RF-A2024001), and the China Postdoctoral Science Foundation (No. 2025M771342).

Author contributions

Gaoan ZHENG, Dapeng TAN, and Xuefeng XU designed the research. Gaoan ZHENG, Xiaoxing WENG, and Pu XU processed the corresponding data. Gaoan ZHENG and Tong WANG wrote the first draft of the manuscript. Xiaoxing WENG and Weixin XU helped to organize the manuscript. Lin LI revised and edited the final version.

Conflict of interest

Gaoan ZHENG, Xiaoxing WENG, Tong WANG, Pu XU, Weixin XU, Lin LI, Xuefeng XU, and Dapeng TAN declare that they have no conflict of interest.

References

Chen J, Ming WW, An QL, et al., 2020. Mechanism and feasibility of ultrasonic-assisted milling to improve the machined

surface quality of 2D C_f/SiC composites. *Ceramics International*, 46(10):15122-15136. https://doi.org/10.1016/j.ceramint.2020.03.047

Chen JT, Ge M, Li L, et al., 2023. Material transport and flow pattern characteristics of gas–liquid–solid mixed flows. *Processes*, 11(8):2254. https://doi.org/10.3390/pr11082254

Deng TT, Zheng ZZ, Li JJ, et al., 2019. Surface polishing of AISI 304 stainless steel with micro plasma beam irradiation. *Applied Surface Science*, 476:796-805. https://doi.org/10.1016/j.apsusc.2019.01.173

Deng TT, Li JJ, Zheng ZZ, 2020. Fundamental aspects and recent developments in metal surface polishing with energy beam irradiation. *International Journal of Machine Tools and Manufacture*, 148:103472. https://doi.org/10.1016/j.ijmachtools.2019.103472

Feng JY, Zhang ZY, Yu SQ, et al., 2023. Novel multiphase jet polishing for complicated structured components produced by laser powder bed fusion. *Additive Manufacturing*, 72: 103634.

Fettiplace R, Haydon DA, 1980. Water permeability of lipid membranes. *Physiological Reviews*, 60(2):510-550. https://doi.org/10.1152/physrev.1980.60.2.510

Finnie I, 1960. Erosion of surfaces by solid particles. *Wear*, 3(2):87-103. https://doi.org/10.1016/0043-1648(60)90055-7

Finnie I, 1972. Some observations on the erosion of ductile metals. *Wear*, 19(1):81-90. https://doi.org/10.1016/0043-1648(72)90444-9

Forder A, Thew M, Harrison D, 1998. A numerical investigation of solid particle erosion experienced within oilfield control valves. *Wear*, 216(2):184-193. https://doi.org/10.1016/S0043-1648(97)00217-2

Fu DN, Sheng J, Wang LJ, et al., 2025. In situ silver-loaded cellulose for high-strength antibacterial composite air filtration paper. *Cellulose*, 32:3375-3388. https://doi.org/10.1007/s10570-025-06448-4

Gao Y, Wu MR, Lin Y, et al., 2020. Acoustic microfluidic separation techniques and bioapplications: a review. *Micromachines*, 11(10):921. https://doi.org/10.3390/mi11100921

Gao YF, Wang YP, Wang YZ, et al., 2023. Nanocatalysis meets microfluidics: a powerful platform for sensitive bioanalysis. *TrAC Trends in Analytical Chemistry*, 158:116887. https://doi.org/10.1016/j.trac.2022.116887

Ge JQ, Ren YL, Li C, et al., 2023. Ultrasonic coupled abrasive jet polishing (UC-AJP) of glass-based micro-channel for micro-fluidic chip. *International Journal of Mechanical Sciences*, 244:108055. https://doi.org/10.1016/j.ijmecsci.2022.108055

Ge JQ, Lin YH, Qi H, et al., 2024. The impact of ultrasonic-induced jet morphology on polishing efficiency. *International Journal of Mechanical Sciences*, 284:109764. https://doi.org/10.1016/j.ijmecsci.2024.109764

Grant G, Tabakoff W, 1975. Erosion prediction in turbomachinery resulting from environmental solid particles. *Journal of Aircraft*, 12(5):471-478. https://doi.org/10.2514/3.59826

Guo XM, Yang MY, Li FQ, et al., 2024. Investigation on cryogenic cavitation characteristics of an inducer considering thermodynamic effects. *Energies*, 17(15):3627. https://doi.org/10.3390/en17153627

Ji RQ, Shen QT, Zhang L, et al., 2024. Novel photocatalysis-assisted mechanical polishing of laser cladding cobalt-based alloy using TiO_2 nanoparticles. *Powder Technology*, 444:119990. https://doi.org/10.1016/j.powtec.2024.119990

Kim G, Denos BR, Sterkenburg R, 2020. Influence of different piercing methods of abrasive waterjet on delamination of fiber reinforced composite laminate. *Composite Structures*, 240:112065. https://doi.org/10.1016/j.compstruct.2020.112065

Kowsari K, Nouraei H, James DF, et al., 2014. Abrasive slurry jet micro-machining of holes in brittle and ductile materials. *Journal of Materials Processing Technology*, 214(9): 1909-1920. https://doi.org/10.1016/j.jmatprotec.2014.04.008

Kumar AS, Deb S, Paul S, 2021. Ultrasonic-assisted abrasive micro-deburring of micromachined metallic alloys. *Journal of Manufacturing Processes*, 66:595-607. https://doi.org/10.1016/j.jmapro.2021.04.019

Li J, Ji SM, Tan DP, 2017. Improved soft abrasive flow finishing method based on turbulent kinetic energy enhancing. *Chinese Journal of Mechanical Engineering*, 30(2):301-309. https://doi.org/10.1007/s10033-017-0071-y

Li K, Zhou XX, Zheng HY, et al., 2022. Achieving full forward flow of valveless piezoelectric micropump used for micro analysis system. *Actuators*, 11(8):218. https://doi.org/10.3390/act11080218

Li L, Lu JF, Fang H, et al., 2020. Lattice Boltzmann method for fluid-thermal systems: status, hotspots, trends and outlook. *IEEE Access*, 8:27649-27675. https://doi.org/10.1109/ACCESS.2020.2971546

Li L, Tan DP, Yin ZC, et al., 2021a. Investigation on the multiphase vortex and its fluid-solid vibration characters for sustainability production. *Renewable Energy*, 175:887-909. https://doi.org/10.1016/j.renene.2021.05.027

Li L, Tan DP, Wang T, et al., 2021b. Multiphase coupling mechanism of free surface vortex and the vibration-based sensing method. *Energy*, 216:119136. https://doi.org/10.1016/j.energy.2020.119136

Li L, Yang YS, Xu WX, et al., 2022. Advances in the multiphase vortex-induced vibration detection method and its vital technology for sustainable industrial production. *Applied Sciences*, 12(17):8538. https://doi.org/10.3390/app12178538

Li L, Tan YF, Xu WX, et al., 2023a. Fluid-induced transport dynamics and vibration patterns of multiphase vortex in the critical transition states. *International Journal of Mechanical Sciences*, 252:108376. https://doi.org/10.1016/j.ijmecsci.2023.108376

Li L, Xu WX, Tan YF, et al., 2023b. Fluid-induced vibration evolution mechanism of multiphase free sink vortex and the multi-source vibration sensing method. *Mechanical*

Systems and Signal Processing, 189:110058. https://doi.org/10.1016/j.ymssp.2022.110058

Li L, Lu B, Xu WX, et al., 2023c. Mechanism of multiphase coupling transport evolution of free sink vortex. *Acta Physica Sinica*, 72(3):034702. https://doi.org/10.7498/aps.72.20221991

Li L, Gu ZH, Xu WX, et al., 2023d. Mixing mass transfer mechanism and dynamic control of gas-liquid-solid multiphase flow based on VOF-DEM coupling. *Energy*, 272: 127015. https://doi.org/10.1016/j.energy.2023.127015

Li L, Li QH, Ni YS, et al., 2024a. Critical penetrating vibration evolution behaviors of the gas-liquid coupled vortex flow. *Energy*, 292:130236. https://doi.org/10.1016/j.energy.2024.130236

Li L, Lu B, Xu WX, et al., 2024b. Dynamic behaviors of multiphase vortex-induced vibration for hydropower energy conversion. *Energy*, 308:132897. https://doi.org/10.1016/j.energy.2024.132897

Li L, Xu P, Xu WX, et al., 2024c. Multi-field coupling vibration patterns of the multiphase sink vortex and distortion recognition method. *Mechanical Systems and Signal Processing*, 219:111624. https://doi.org/10.1016/j.ymssp.2024.111624

Li L, Xu P, Li QH, et al., 2025a. A coupled LBM-LES-DEM particle flow modeling for microfluidic chip and ultrasonic-based particle aggregation control method. *Applied Mathematical Modelling*, 143:116025. https://doi.org/10.1016/j.apm.2025.116025

Li L, Xu P, Li QH, Yin ZC, et al., 2025b. Multi-field coupling particle flow dynamic behaviors of the microreactor and ultrasonic control method. *Powder Technology*, 454: 120731. https://doi.org/10.1016/j.powtec.2025.120731

Li QH, Xu P, Li L, et al., 2024. Investigation on the lubrication heat transfer mechanism of the multilevel gearbox by the lattice Boltzmann method. *Processes*, 12(2):381. https://doi.org/10.3390/pr12020381

Li Z, Wang CY, Li L, et al., 2024. Numerical investigation of mesoscale multiphase mass transport mechanism in fibrous porous media. *Engineering Applications of Computational Fluid Mechanics*, 18(1):2363246. https://doi.org/10.1080/19942060.2024.2363246

Li ZA, Ge JQ, Li X, et al., 2024. Numerical and experimental study on cavitation enhancement of ultrasonic coupled abrasive jet polishing. *The International Journal of Advanced Manufacturing Technology*, 131(12):5769-5786. https://doi.org/10.1007/s00170-024-13253-z

Li ZH, Zheng X, 2014. The problems and progress in the experimental study of micro/nano-scale flow. *Journal of Experiments in Fluid Mechanics*, 28(3):1-11 (in Chinese). https://doi.org/10.11729/syltlx20140018

Lin H, Ma M, Qi H, et al., 2025a. 3D-printed photocatalysts for revolutionizing catalytic conversion of solar to chemical energy. *Progress in Materials Science*, 151:101427. https://doi.org/10.1016/j.pmatsci.2025.101427

Lin H, Shen QT, Ma M, et al., 2025b. 3D printing of porous ceramics for enhanced thermal insulation properties. *Advanced Science*, 12(7):2412554. https://doi.org/10.1002/advs.202412554

Liu XH, Zhao CY, Su GS, et al., 2024. Enhanced fabrication of conical array via two-stage through mask electrochemical machining process. *International Journal of Electrochemical Science*, 19:100614. https://doi.org/10.1016/j.ijoes.2024.100614

Lu JF, Wang T, Li L, et al., 2020. Dynamic characteristics and wall effects of bubble bursting in gas-liquid-solid three-phase particle flow. *Processes*, 8(7):760. https://doi.org/10.3390/pr8070760

Ma YG, Liu CB, Cao SY, et al., 2023. Microfluidics for diagnosis and treatment of cardiovascular disease. *Journal of Materials Chemistry B*, 11(3):546-559. https://doi.org/10.1039/D2TB02287G

Mofakham AA, Ahmadi G, 2020. On random walk models for simulation of particle-laden turbulent flows. *International Journal of Multiphase Flow*, 122:103157. https://doi.org/10.1016/j.ijmultiphaseflow.2019.103157

Nakamura T, Kawai M, Sato Y, et al., 2020. The effect of size and charge of lipid nanoparticles prepared by microfluidic mixing on their lymph node transitivity and distribution. *Molecular Pharmaceutics*, 17(3):944-953. https://doi.org/10.1021/acs.molpharmaceut.9b01182

O'Neill LE, Mudawar I, 2020. Review of two-phase flow instabilities in macro- and micro-channel systems. *International Journal of Heat and Mass Transfer*, 157:119738. https://doi.org/10.1016/j.ijheatmasstransfer.2020.119738

Painuly M, Singh RP, Trehan R, 2023. Electrochemical machining and allied processes: a comprehensive review. *Journal of Solid State Electrochemistry*, 27(12):3189-3256. https://doi.org/10.1007/s10008-023-05610-x

Peng YF, Shen BY, Wang ZZ, et al., 2021. Review on polishing technology of small-scale aspheric optics. *The International Journal of Advanced Manufacturing Technology*, 115(4):965-987. https://doi.org/10.1007/s00170-021-07202-3

Qi H, Qin SK, Cheng ZC, et al., 2021. Towards understanding performance enhancing mechanism of micro-holes on K9 glasses using ultrasonic vibration-assisted abrasive slurry jet. *Journal of Manufacturing Processes*, 64: 585-593. https://doi.org/10.1016/j.jmapro.2021.01.048

Ramshani Z, Zhang CG, Richards K, et al., 2019. Extracellular vesicle microRNA quantification from plasma using an integrated microfluidic device. *Communications Biology*, 2:189. https://doi.org/10.1038/s42003-019-0435-1

Shan J, Guo LH, Ran PH, et al., 2022. Implantable double-layer pump chamber piezoelectric valveless micropump with adjustable flow rate function. *Journal of Micromechanics and Microengineering*, 32(10):105002. https://doi.org/10.1088/1361-6439/ac8099

Shanu A, Sharma P, Dixit P, 2024. Micromachining of alumina ceramic for microsystems applications: a systematic review, challenges and future opportunities. *Materials and Manufacturing Processes*, 39(7):892-924. https://doi.org/10.1080/10426914.2023.2290244

Sheikholeslami M, Jafaryar M, Li ZX, 2018. Nanofluid turbulent convective flow in a circular duct with helical turbulators considering CuO nanoparticles. *International Journal of Heat and Mass Transfer*, 124:980-989. https://doi.org/10.1016/j.ijheatmasstransfer.2018.04.022

Shin YC, Wu BX, Lei ST, et al., 2020. Overview of laser applications in manufacturing and materials processing in recent years. *Journal of Manufacturing Science and Engineering*, 142(11):110818. https://doi.org/10.1115/1.4048397

Subramani K, Vasudevan A, Karthik K, et al., 2022. Insights of abrasive water jet polishing process characteristics and its advancements. *Materials Today: Proceedings*, 52:1113-1120. https://doi.org/10.1016/j.matpr.2021.11.005

Sun XM, Dong X, Wang KD, et al., 2024. Femtosecond laser processing of controlled tapered micro-holes based on dynamic control of relative attitude. *Optics & Laser Technology*, 170:110201. https://doi.org/10.1016/j.optlastec.2023.110201

Tadaki D, Yamaura D, Araki S, et al., 2017. Mechanically stable solvent-free lipid bilayers in nano- and micro-tapered apertures for reconstitution of cell-free synthesized hERG channels. *Scientific Reports*, 7(1):17736. https://doi.org/10.1038/s41598-017-17905-x

Tan DP, Li L, Zhu YL, et al., 2019. Critical penetration condition and Ekman suction-extraction mechanism of a sink vortex. *Journal of Zhejiang University-SCIENCE A*, 20(1):61-72. https://doi.org/10.1631/jzus.A1800260

Tan DP, Li L, Yin ZC, et al., 2020. Ekman boundary layer mass transfer mechanism of free sink vortex. *International Journal of Heat and Mass Transfer*, 150:119250. https://doi.org/10.1016/j.ijheatmasstransfer.2019.119250

Tan YF, Ni YS, Xu WX, et al., 2023. Key technologies and development trends of the soft abrasive flow finishing method. *Journal of Zhejiang University-SCIENCE A*, 24(12):1043-1064. https://doi.org/10.1631/jzus.A2300038

Tan YF, Ni YS, Wu JF, et al., 2024. Machinability evolution of gas-liquid-solid three-phase rotary abrasive flow finishing. *The International Journal of Advanced Manufacturing Technology*, 131(5-6):2145-2164. https://doi.org/10.1007/s00170-022-10761-8

Tarodiya R, Levy A, 2021. Surface erosion due to particle-surface interactions–a review. *Powder Technology*, 387:527-559. https://doi.org/10.1016/j.powtec.2021.04.055

Tong WJ, Li L, 2024. Experimental research of ultrasonic cavitation evolution mechanism and model optimization of RUREMM on cylindrical surface. *Processes*, 12(5):884. https://doi.org/10.3390/pr12050884

Turkyilmazoglu M, Alofi AS, 2024. Liquid vortex formation in a swirling container considering fractional time derivative of Caputo. *Fractal and Fractional*, 8(4):231. https://doi.org/10.3390/fractalfract8040231

Wang CY, Li Z, Xu P, et al., 2025. Collision modeling approach and transient response mechanism of ring-ribbed cylindric shells for underwater vehicles. *Applied Mathematical Modelling*, 141:115923. https://doi.org/10.1016/j.apm.2024.115923

Wang T, Wang CY, Yin YX, et al., 2023. Analytical approach for nonlinear vibration response of the thin cylindrical shell with a straight crack. *Nonlinear Dynamics*, 111(12):10957-10980. https://doi.org/10.1007/s11071-023-08460-4

Wang T, Tan DP, Hou YQ, et al., 2025. Analytical and experimental investigation of vibration response for the cracked fluid-filled thin cylindrical shell under transport condition. *Applied Mathematical Modelling*, 142:115969. https://doi.org/10.1016/j.apm.2025.115969

Wu JF, Li L, Yin ZC, et al., 2024a. Mass transfer mechanism of multiphase shear flows and interphase optimization solving method. *Energy*, 292:130475. https://doi.org/10.1016/j.energy.2024.130475

Wu JF, Xu P, Li L, et al., 2024b. Multiphase dynamic interfaces and abrasive transport dynamics for abrasive flow machining in shear thickening transition states. *Powder Technology*, 446:120150. https://doi.org/10.1016/j.powtec.2024.120150

Xiao H, Dai YF, Duan J, et al., 2021. Material removal and surface evolution of single crystal silicon during ion beam polishing. *Applied Surface Science*, 544:148954. https://doi.org/10.1016/j.apsusc.2021.148954

Xu P, Li QH, Wang CY, et al., 2025. Interlayer healing mechanism of multipath deposition 3D printing models and interlayer strength regulation method. *Journal of Manufacturing Processes*, 141:1031-1047. https://doi.org/10.1016/j.jmapro.2025.03.062

Xu WX, Xu P, Yang Y, et al., 2025. The utilization and advancement of laser ultrasound testing in the assessment of aerospace composite characteristics: a review. *Chinese Journal of Aeronautics*, 38(12):103789. https://doi.org/10.1016/j.cja.2025.103789

Yan Q, Fan XH, Li L, et al., 2024. Investigations of the mass transfer and flow field disturbance regulation of the gas-liquid-solid flow of hydropower stations. *Journal of Marine Science and Engineering*, 12(1):84. https://doi.org/10.3390/jmse12010084

Yan QF, Sun WT, Zhang L, et al., 2021. Effects of vibration characteristics on the atomization performance in the medical piezoelectric atomization device induced by intra-hole fluctuation. *Chinese Journal of Mechanical Engineering*, 34(1):123. https://doi.org/10.1186/s10033-021-00635-7

Yang X, Zhang ZY, Zhang TC, et al., 2024. Multi-build orientation effects on microstructural evolution and mechanical behavior of truly as-built selective laser melting Ti6Al4V alloys. *Journal of Materials Research and Technology*, 30:3967-3976. https://doi.org/10.1016/j.jmrt.2024.04.031

Yin ZC, Lu JF, Li L, et al., 2020. Optimized scheme for accelerating the slagging reaction and slag–metal–gas emulsification in a basic oxygen furnace. *Applied Sciences*, 10(15):5101. https://doi.org/10.3390/app10155101

Yin ZC, Ni YS, Li L, et al., 2024. Numerical modeling and experimental investigation of a two-phase sink vortex and its fluid-solid vibration characteristics. *Journal of Zhejiang University-SCIENCE A*, 25(1):47-62. https://doi.org/10.1631/jzus.A2200014

Zhang CX, Xu ZY, Zhang XY, et al., 2020. Surface integrity of holes machined by electrochemical discharge drilling method. *CIRP Journal of Manufacturing Science and Technology*, 31:643-651. https://doi.org/10.1016/j.cirpj.2020.09.004

Zhang F, Huang X, Chen BC, et al., 2022. Research on the machinability of micro-tapered hole group in piezoelectric atomizer and the improvement method. *Sensors*, 22(20): 7891. https://doi.org/10.3390/s22207891

Zhang HS, Tan DP, Xu SC, et al., 2024. Investigation of crack propagation and failure of liquid-filled cylindrical shells damaged in high-pressure environments. *Journal of Marine Science and Engineering*, 12(6):921. https://doi.org/10.3390/jmse12060921

Zhang YK, Li Z, Li L, et al., 2025. Deposition mechanism of microscopic impacting droplets on flexible porous substrates. *International Journal of Mechanical Sciences*, 288:110050. https://doi.org/10.1016/j.ijmecsci.2025.110050

Zhao J, Jiang EY, Qi H, et al., 2020. A novel polishing method for single-crystal silicon using the cavitation rotary abrasive flow. *Precision Engineering*, 61:72-81. https://doi.org/10.1016/j.precisioneng.2019.10.002

Zheng GA, Gu ZH, Xu WX, et al., 2023a. Gravitational surface vortex formation and suppression control: a review from hydrodynamic characteristics. *Processes*, 11(1):42. https://doi.org/10.3390/pr11010042

Zheng GA, Shi JL, Li L, et al., 2023b. Fluid-solid coupling-based vibration generation mechanism of the multiphase vortex. *Processes*, 11(2):568. https://doi.org/10.3390/pr11020568

Zheng GA, Xu P, Li L, et al., 2024. Investigations of the formation mechanism and pressure pulsation characteristics of pipeline gas-liquid slug flows. *Journal of Marine Science and Engineering*, 12(4):590. https://doi.org/10.3390/jmse12040590

Zheng GA, Xu P, Li L, 2025a. Investigate on the fluid dynamics and heat transfer behavior in an automobile gearbox based on the LBM-LES model. *Lubricants*, 13(3):117. https://doi.org/10.3390/lubricants13030117

Zheng GA, Xu P, Wang T, et al., 2025b. Study on the bubble collapse characteristics and heat transfer mechanism of the microchannel reactor. *Processes*, 13(1):281. https://doi.org/10.3390/pr13010281